Engineering Structures 362 (2026) 123003

Contents lists available at ScienceDirect

Engineering Structures

journal homepage: www.elsevier.com/locate/engstruct

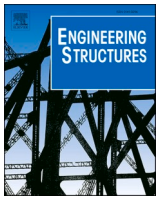

Incipient damage localization in thick-walled hollow cylinders based on nonlinear elastic wave scattering features

Yuanman Zhang [a,b], Shengbo Shan [c,d,*], Li Cheng [a,b,**]

[a] Department of Mechanical Engineering, The Hong Kong Polytechnic University, Kowloon, Hong Kong
[b] Hong Kong Branch of National Rail Transit Electrification and Automation Engineering Technology Research Center, The Hong Kong Polytechnic University, Kowloon, Hong Kong
[c] College of Intelligence Science and Technology, National University of Defense Technology, Changsha 410073, PR China
[d] National Key Laboratory of Equipment State Sensing and Smart Support, National University of Defense Technology, Changsha 410073, PR China

ARTICLE INFO

Keywords:
Nonlinear elastic waves
Incipient damage
Damage localization
Thick-walled hollow cylinder

ABSTRACT

Thick-walled hollow cylinders (TWHCs) are widely used in engineering structures and transportation systems, exemplified by train axles. The early detection and precise localization of incipient damage in such structures is of great significance for maintaining structural integrity and operational safety. In existing technologies, methods based on nonlinear elastic waves exhibit high sensitivity in detecting incipient damage, but due to insufficient understanding of nonlinear wave-damage interactions, progress in localization has been very limited. Previous investigations have revealed that the interaction between quasi-surface waves and incipient damage in a TWHC produces strongly directional nonlinear wave scattering. Building on this physical insight, this paper establishes a strategy for damage localization in a TWHC. The proposed method starts with the definition of an effective detection zone (EDZ) for each sensor placed along the inner the surface of a TWHC, followed by the construction of a network-level detection zone through the merging of multiple EDZs. The nonlinear parameter variation (NPV) of each sensor is quantified and incorporated as a weighting factor in *Softmax* algorithm. This zone-aware and sensor-weighted strategy significantly improves the accuracy and the robustness of damage localization. Numerical analyses and experiments confirm the effectiveness of the proposed method, pointing out its great potential in applications such as early damage detection/localization of train axles.

1. Introduction

Thick-walled hollow cylinders (TWHCs) are widely used as major load-bearing structures in mechanical and transportation systems, such as train axles [1]. During operation, structural damage, such as cracks and corrosions, etc., can initiate and evolve, which may eventually jeopardize the safe operation of the system or even lead to catastrophic failure. Prior to the occurrence of macroscale damage, materials usually undergo a continuous degradation process. Alongside this is the generation of microscale or often invisible damage, referred to as incipient damage, which manifests as the precursor of more visible macroscale damage. For metal TWHCs, this process is closely tied with the plastic deformation in metals formed under continuous tensile and compressive stresses. Therefore, successful localization of the occurrence of such incipient damage can significantly shift the maintenance schedule to an earlier stage which in turn increases the operational safety of the structures [2–5].

As a higher level of structural health management, damage localization is more demanding than detection. For the former, rather mature methods have been developed based on linear elastic wave-based structural health monitoring (SHM) techniques [6–10]. For example, damage diagnostic imaging algorithms [11,12] are particularly favored due to their ability to provide interpretable and intuitive visual damage locations. Some representative algorithms are phase arrays approach [13,14], tomography technique [15–17], probability-based diagnostic imaging method [12,18,19], and delay-and-sum algorithm [20–22]. In hollow cylindrical structures, damage localization differs from that in plates due to the presence of helical guided waves, which have been widely studied [23–25]. For example, Zhu et al. proposed a helical sensor network for internal damage localization in large-scale hollow

* Corresponding author at: College of Intelligence Science and Technology, National University of Defense Technology, Changsha 410073, PR China.
** Corresponding author at: Department of Mechanical Engineering, The Hong Kong Polytechnic University, Kowloon, Hong Kong.
E-mail addresses: shanshengbo25@nudt.edu.cn (S. Shan), li.cheng@polyu.edu.hk (L. Cheng).

https://doi.org/10.1016/j.engstruct.2026.123003
Received 22 September 2025; Received in revised form 11 April 2026; Accepted 15 May 2026

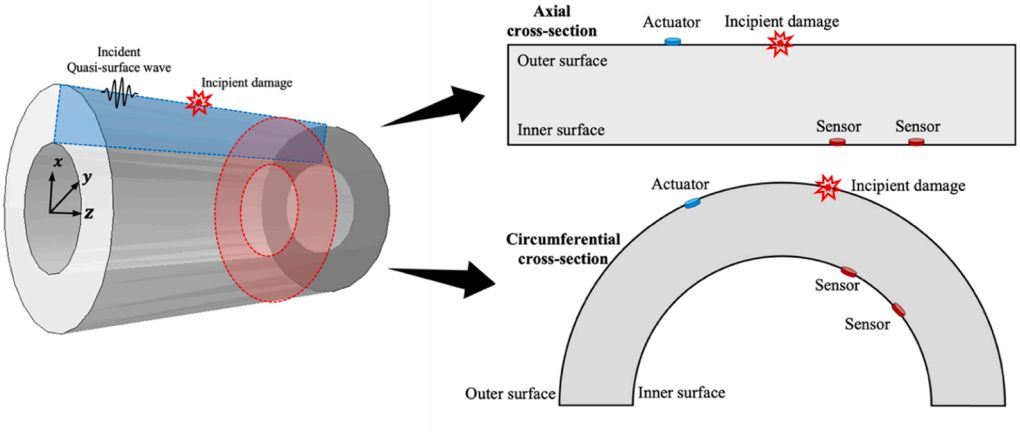

Fig. 1. Sketch of a TWHC with axial and circumferential cross-sections.

cylinders, demonstrating that helical wave-based sensing can provide flexible propagation paths and effective coverage for reliable damage detection [26]. Hu et al. developed a Bayesian hierarchical hyper-Laplacian prior-based imaging method for pipe structures, demonstrating its capability to enhance imaging resolution and improve defect localization accuracy through sparse reconstruction [27]. However, these methods have been predominantly applied to the detection and localization of macroscale damage due to the causality limitation in terms of wavelength versus damage size. Such macroscale damage differs significantly from the incipient damage associated with material nonlinearity, which is presumably much less visible, less intrusive to wave scattering, and therefore more difficult to be detected. To address this challenge, nonlinear ultrasonic techniques [28–31] have been exploited. For instance, tomography has been applied to the nonlinear regime by synthesizing damage information from multiple actuator-sensor paths [32]. The wave mixing technique has also been used for incipient damage localization [33]. By tuning and controlling the location of the mixing zone of a pair of guided waves, zone-by-zone damage detection has been achieved using nonlinear Lamb waves.

Note the aforementioned nonlinear localization methods have mainly been designed for thin-walled structures like plates. These methods, in principle, cannot be directly applied to thick-walled structures like TWHCs, mainly due to several reasons. First, the scattering nonlinear signals induced by incipient damage are relatively weak, making them difficult to extract and more likely to be obscured by the linear components which usually are much more dominant in energy level. Second, it is difficult to obtain accurate time information from these nonlinear signals to inform on the location of incipient damage. Additionally, wave propagation in thick-walled structures is complex, bearing multiple modes [34,35], which significantly increases the difficulty in apprehending and using nonlinear elastic waves.

Recently, a new nonlinear elastic wave scattering phenomenon has been discovered in our previous work [36], which offers new possibilities for incipient damage localization. The reported wave scattering results from the interaction between elastic waves and a specific zone with material nonlinearity. Furthermore, variations in wall thickness and damage size in thick-walled structures have minimal effect on the scattering angle. Although this finding has been confirmed in two-dimensional (2D) cases, it is unclear whether 3D localization is possible due to the foreseeable increasing complexity of wave propagation and scattering in the presence of incipient damage. Therefore, it is crucial to investigate the issue to gain a deeper understanding of the incipient damage-induced scattering characteristics of the newly discovered second harmonic elastic waves and ascertain how the findings can be leveraged to achieve damage localization through proper design of sensor configuration. Meanwhile, most methods for simulating incipient damage in both experimental and simulation contexts involve the modification of local material properties by techniques such as heating [37–40], stamping [36], or tensile loading [41,42]. However, replicating adjustable and controllable incipient damage in structures is usually difficult. Motivated by these, this work is carried out with a twofold objective, thus showing its novelty: 1) to investigate the wave-damage interaction in a 3D TWHC and 2) to establish a dedicated algorithm for incipient damage localization thorough numerical analyses and experimental validations by controlling a localized nonlinear scatterer mimicking incipient damage in the TWHC.

Targeting these goals, this work carries out a comprehensive study on incipient damage localization methods based on the understanding of the nonlinear elastic wave propagation in TWHCs. The influence of structural curvature on the nonlinear elastic wave propagation is first evaluated. Then, through the mapping relationships of sensors on the inner and outer surfaces of TWHCs, the area covered by each sensor is determined, and the probability of damage occurrence in these regions is quantified. In light of the scattering properties of nonlinear elastic waves, a sensor network is designed, along with the proposal of a dedicated localization algorithm. The efficacy of both the sensor layout and the damage localization algorithm is validated through numerical analyses and experiments.

2. Nonlinear elastic wave propagation in TWHC

We examine a thick-walled hollow cylinder (TWHC) as shown in Fig. 1. The structure would represent a simplified train axle model, featuring a hollow shaft with a thick wall. The outer surface of the TWHC is deemed more vulnerable to incipient damage associated with material nonlinearity, typically induced by impact, fatigue, or corrosion. Quasi-surface waves are to be used to detect such damage. To this end, a detection scheme is considered where an actuator is placed on the outer surface, while receiving sensors are mounted on the inner surface for practical reasons. The actuator generates quasi-surface waves that, upon interacting with damage, produce nonlinear waves, which subsequently scatter inward into the structure.

Building on this detection setting, a comprehensive understanding of the wave propagation and scattering characteristics in such structures is essential for conceiving proper damage localization strategies. Due to the curved geometry of the TWHC, the analysis must account not only for scattering patterns in a two-dimensional cross-sectional plane but also for the influence of curvature on the propagation path, energy distribution, and scattering modes of nonlinear waves. Accordingly, we divide the TWHC into two primary study domains: the axial cross-section and the circumferential cross-section, as shown in Fig. 1. For each case, the scattering features of nonlinear waves generated by

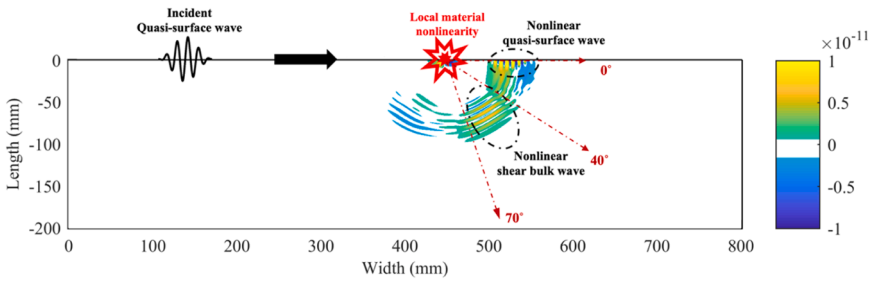

Fig. 2. Sketch of the nonlinear elastic wave scattering features caused by local material nonlinearity in the cross-section of a thick-walled hollow cylinder.

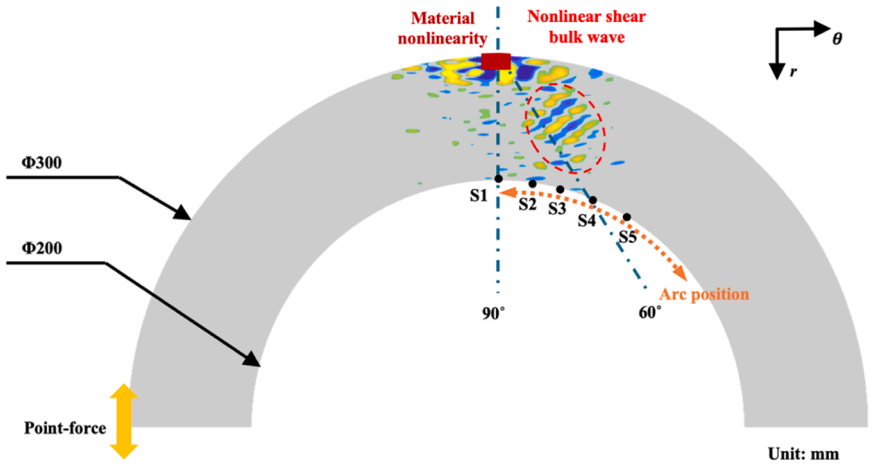

Fig. 3. Sketch of the scattered nonlinear elastic wave on the curved surface.

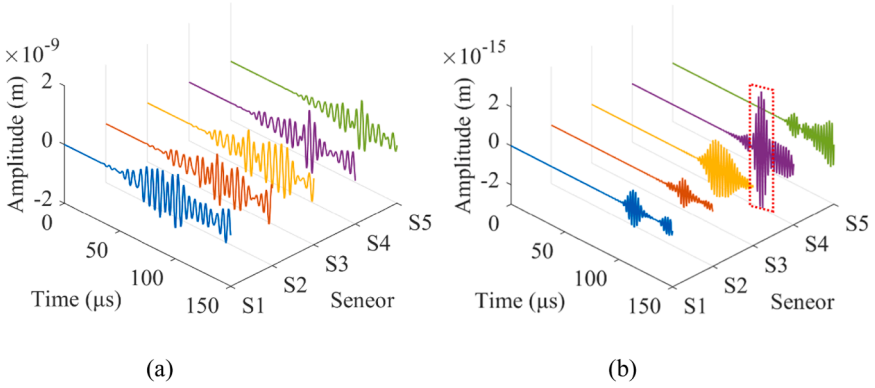

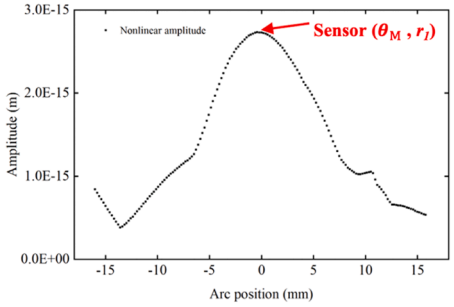

Fig. 4. (a) Linear and (b) nonlinear responses captured by sensors S1-S5, (c) scattering distribution of nonlinear shear bulk wave on the inner surface.

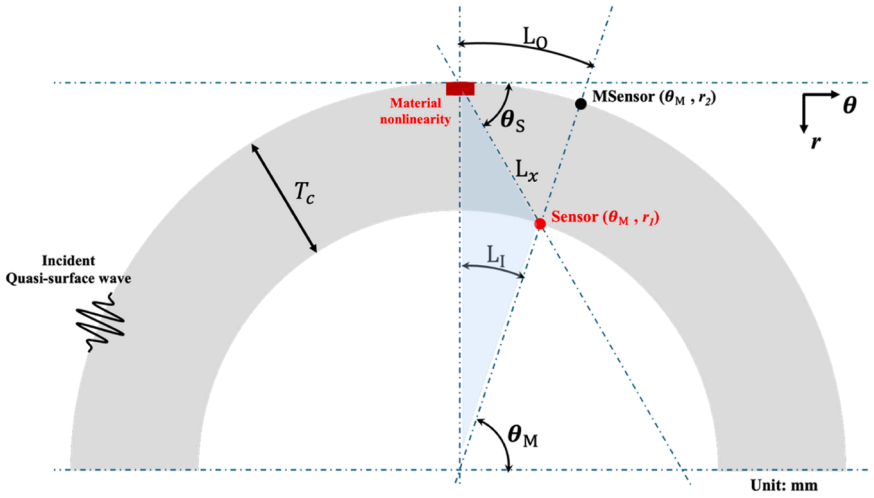

Fig. 5. Sketch of inner-outer surface sensor mapping.

localized nonlinear material regions are investigated.

Our previous work [36] demonstrated that, under a tone burst excitation, the local material nonlinear region acts as a secondary wave source to generate second harmonic waves that propagate along the structural surface and penetrate towards the interior of the structure, referred to as nonlinear quasi-surface waves and bulk waves, respectively. It was found that the nonlinear shear bulk waves scatter towards the interior of the thick-walled structure, with the dominant scattering angle ranging between 40° and 70°, as sketched in Fig. 2, which shows an axial cross-section of the TWHC. Parametric studies also showed that the scattering angle is not sensibly affected by the size or the shape of the nonlinear material zone. In addition, the energy of the nonlinear quasi-surface wave is mainly confined near the surface after interacting with the local material nonlinearity. The nonlinear shear bulk waves are generated by the interaction between the incident waves and the nonlinear material region. Since the material under consideration is isotropic, the higher order elastic constants that characterize the extent of material nonlinearity mainly affect the amplitude of the generated nonlinear shear waves. By contrast, the directivity of the generated nonlinear waves is more related to the wave structure of incident waves.

Prior to the development of incipient damage localization method, the influence of the structural curvature on the nonlinear elastic wave propagation is evaluated. To this end, a semi-circular structural mode is established in Abaqus/Explicit. The inner and outer diameters are 200 mm and 300 mm, respectively. Plane strain elements (CPE4) are used with a mesh size of 0.5 mm × 0.5 mm, corresponding to approximately 14 elements per smallest wavelength of interest. The excitation is applied as a prescribed circumferential displacement using a 5-cycle tone burst at 200 kHz, simulating the effect of a surface-mounted actuator. Five sensors are placed on the inner surface of the structure with an angular interval of 10°, whose positions are marked in Fig. 3. Each sensor is designed to capture the circumferential displacement centered at the local material nonlinear region. Sensor S1 is located directly below the damage zone, with an arc length of 19 mm away from S4. Specifically, the second harmonic responses, captured at different sensing positions, are extracted with the phase-inverse method [43] to eliminate the linear components.

The linear and nonlinear responses captured by sensors S1–S5 in terms of the circumferential displacement are shown in Fig. 4. It can be observed that the linear signal (which should be the global signal largely dominated by linear components) is rather irregular without clear propagation pattern. In contrast, the nonlinear signal displays distinctive scattering characteristics. Fig. 4(b) reveals that the nonlinear signal intensity received by sensor S4, positioned at an angle of 60° relative to the damaged area, is overwhelmingly stronger than the others. Upon calculating the propagation time, the wave packet at around 100 μs marked by red dotted box for sensor S4 corresponds to the nonlinear shear bulk wave. Meanwhile, the nonlinear shear bulk wave scatter inward toward the inner surface, with a primary scattering angle of approximately 60°, as shown in Fig. 3. The circumferential case in Fig. 3 aims to demonstrate that the scattering characteristics of nonlinear waves are independent of structural curvature. Based on the wave propagation features, the incipient damage localization method is designed to identify damage on the outer surface of the TWHC.

Focusing on S4, the amplitudes of the nonlinear waves within a range of 19 mm are extracted, resulting in the intensity distribution of the scattering waves on the inner surface, as shown in Fig. 4(c). In this figure, the origin (0 mm) corresponds to the position of S4. It can be seen that the scattering waves have the maximum intensity at S4 position and the scattered nonlinear energy decreases with the scattering distance and scattering angle. This scattering characteristic confirms that the structural curvature has little influence on the scattering features of nonlinear shear bulk waves in terms of the scattering angle. Notably, the scattering angle remains predominantly around 60°. This feature will be capitalized to derive the subsequent damage localization method.

3. 3D incipient damage localization strategy

Based on the above understanding, a 3D incipient damage localization strategy is proposed. First, an effective detection zone (EDZ) on the outer surface is constructed for a specific sensor, using the mapped scattering relationship between the inner and outer surfaces of the TWHC. Then, the fundamental principle of the localization approach, which relies on the second harmonic components of nonlinear elastic waves, is introduced. Finally, the corresponding localization algorithm is presented in detail.

3.1. Mapping relation between inner and outer surfaces

Based on the nonlinear wave scattering features, the layout of the transducers is designed by positioning actuators on the outer surface and sensors on the inner surface of the TWHC. This allows to transmit information of damage on the outer surface to the sensors on the inner surface through the scattered nonlinear shear waves. In this regard, the scattering angles play a pivotal role in guiding the layout design of the sensors on the inner surface.

Given the scattering features of nonlinear bulk waves, the effective detection range of each sensor is first determined, as sketched in Fig. 5. Specifically, a sensor on the inner surface, labeled as *Sensor* (θ_M, r_1), is first mapped onto the outer surface as *MSensor* (θ_M, r_2) using polar

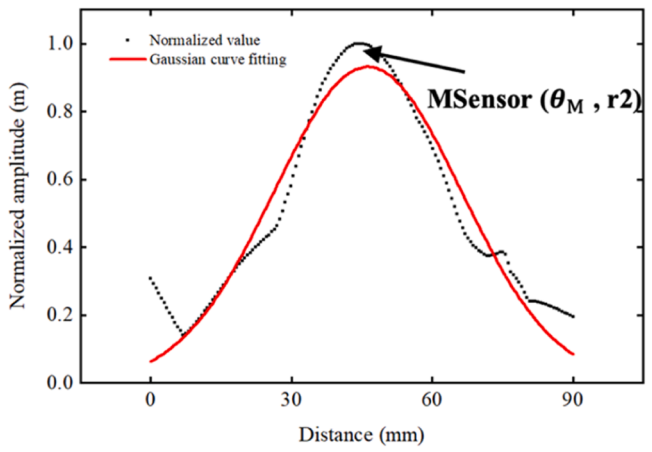

Fig. 6. Effective detection zone and Gaussian fitting on the outer surface along scattering distance.

coordinates. In this polar coordinate system, θ_M represents the angle corresponding to the location of the sensors, while r_1 and r_2 represent the inner and outer radii of the hollow cylinder, respectively. According to the angle corresponding to the strongest scattering amplitude θ_S, the effective detection ranges are determined as L_O and L_I for the outer and inner surfaces respectively. L_x represents the length of scattering path. In the present case, the scattering angle θ_S is set to 60°, and r_1 and r_2 are 100 mm and 150 mm, respectively. Accordingly, L_O and L_I are determined as 49 mm and 19 mm, respectively. Fig. 5 provides a schematic illustration of the inner-outer surface mapping to elucidate the damage localization algorithm.

Based on the mapping relations, the scattering feature of the nonlinear waves in Fig. 4(c), is mapped to the outer surface with the damage zone center as the origin in Fig. 7. After normalization with respect to the maximum amplitude of the captured nonlinear wave signals, a Gaussian fitting is applied to approximate the scattering pattern (P_G) as [44]

$$P_G = 0.9758e^{\left(-\left(\frac{x-L_O}{0.2314}\right)^2\right)} \quad (1)$$

where x is the arc distance between the center of the damage and a mapped location on the outer surface. Using the mapped scattering relationship in Fig. 6, an effective detection zone (EDZ) for a specific sensor on the outer surface is constructed in Fig. 7 in terms of the possibility of damage localization. It indicates that the sensor at the position with high possibility is more likely to capture the damage information. The definition of EDZ will be further utilized in the proposed damage localization algorithm. The EDZ is defined over a finite angular and spatial range, rather than a single deterministic direction. As such, moderate deviations in the scattering angle due to material variability or experimental uncertainty lead only to limited shifts in the EDZ, while the overall spatial coverage remains largely preserved. The Gaussian function is adopted as a convenient and physically reasonable approximation of the observed nonlinear scattering intensity distribution, which exhibits a smooth decay away from the dominant scattering direction.

3.2. Principle of incipient damage localization

In practice, the outer surface of a TWHC is more vulnerable to damage. The inspection zone therefore primarily targets the outer surface based on the scattering properties of the nonlinear bulk waves. As illustrated in Fig. 8, assuming that the incipient damage is located on the outer surface of a hollow cylinder, the damage-induced nonlinear shear bulk waves will be captured by *Sensors* located on the inner surface. The temporal information and energy of the scattering waves are then extracted from the captured signals. By synthesizing this information with the definition of EDZ, incipient damage can be localized.

In practice, actuators are permanently installed at fixed positions. Even though multiple sensors are required, the physical system is still simple without the need of switching actuators and sensors to form a complex network. As damage localization is conducted on the outer surface, it is unfolded into a 2D plane. Similarly, the sensors on the inner surface (*Sensor*) are mapped onto the outer surface as virtual sensor

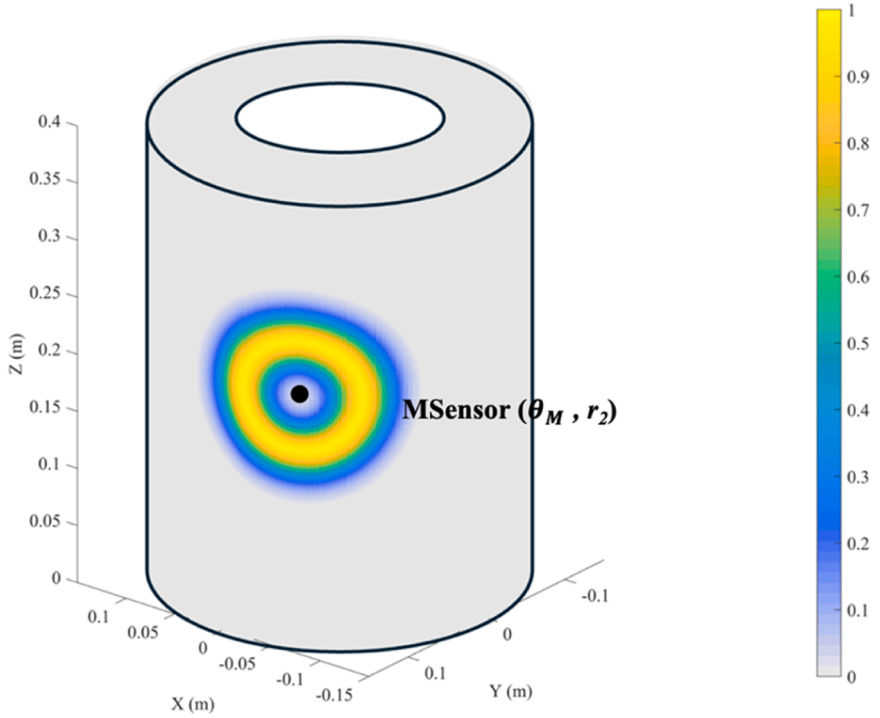

Fig. 7. Spatial distribution of effective detection zone on the outer surface of the TWHC.

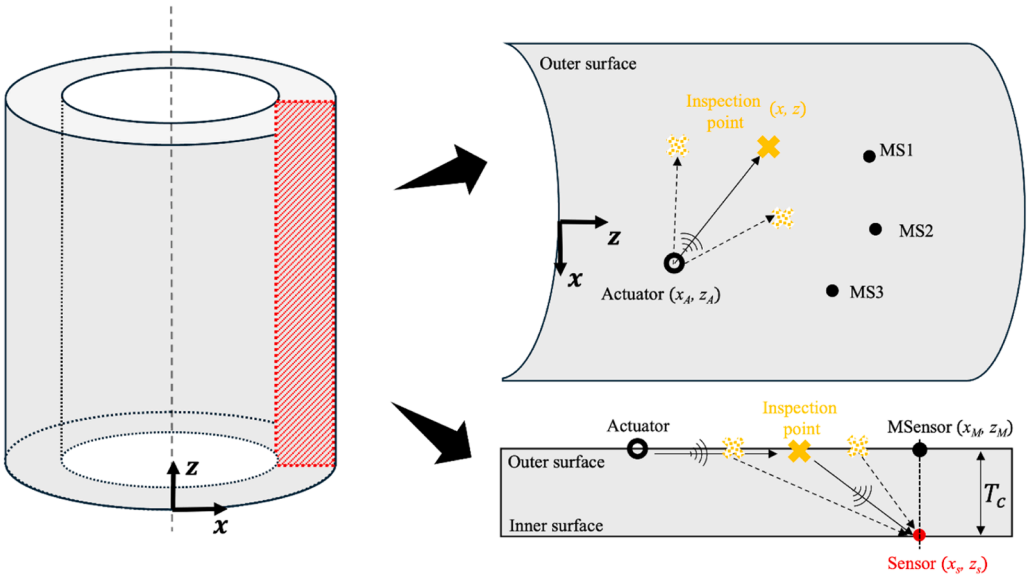

Fig. 8. Localization strategy for the combination of inner and outer surfaces.

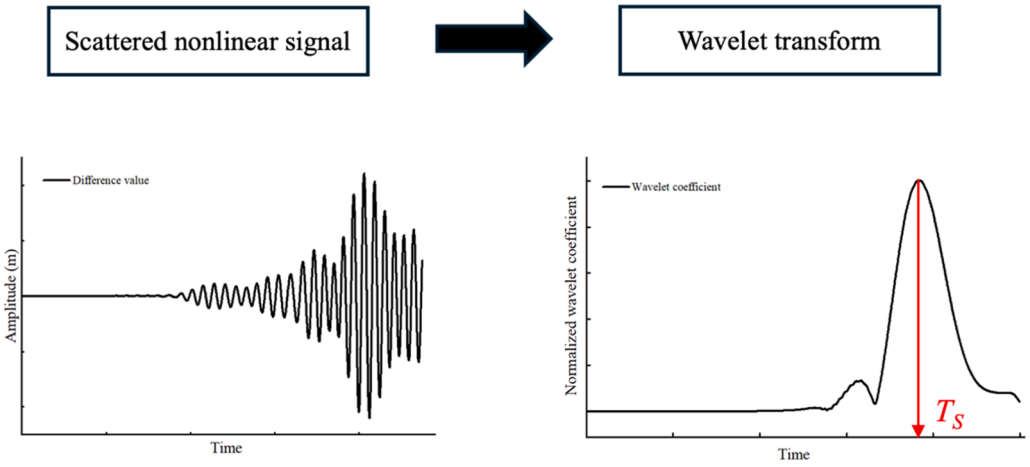

Fig. 9. Arrival time of damage-scattered signal extraction method.

(*MSensor*) via their polar coordinates, as illustrated by MS1, MS2, MS3, etc. in Fig. 8.

3.3. Damage localization algorithm

After illustrating the principle of the damage localization, a dedicated algorithm is proposed to implement the strategy with the following steps. The coordinate system is first defined, with the origin positioned at the boundary on the outer surface of the cylinder, as shown in Fig. 8.

1) Determining the effective detection zone (EDZ)

According to its definition, the EDZ of each sensor i is determined as a circle with a radius of $2L_O$, centered at the location of the *MSensor* (x_M, z_M). Given an inspection point (x, z) on the unfolded outer surface, the distance from this point to a specific *MSensor* is denoted as D. If the point is within the EDZ, the probability of damage detection is defined as P_{EDZ}. Conversely, if the point is located outside the EDZ, P_{EDZ} is considered to be zero. Consequently, P_{EDZ} is defined as

$$P_{EDZ} = \begin{cases} 0.9758e^{\left(-\left(\frac{D-L_O}{0.2314}\right)^2\right)}, & D \le 2L_O \#\#\#\#\#\#\#\# \\ 0, & D > 2L_O \end{cases} \quad (2)$$

2) Extracting temporal information of incipient damage-induced scattering waves

The nonlinear signals captured by sensors are extracted with the phase-inverse method [43] from both damaged and intact samples. Subsequently, the damage-induced nonlinear signals induced by the incipient damage are extracted by subtracting the intact signals from the damaged signals. Complex Morlet wavelet transform [45,46] is then applied to the damage-induced nonlinear signal and the wavelet coefficients are calculated at the instantaneous frequency of the nonlinear signal. It provides a well-balanced time-frequency resolution, enabling precise identification of the wave packet associated with the second harmonic while maintaining robustness against noise. In addition, the wavelet coefficients allow for a clear determination of the signal energy distribution in the time-frequency domain, from which the arrival time can be reliably extracted as the point of maximum response at the target

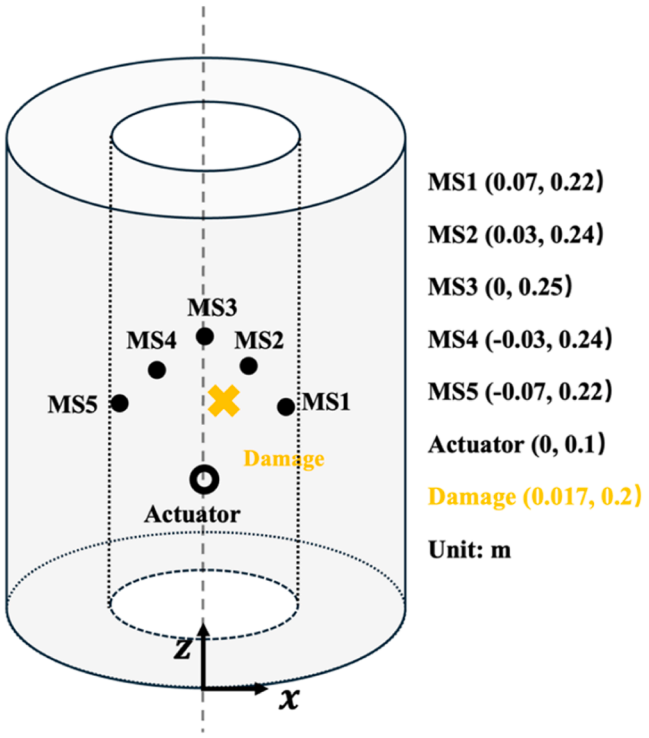

Fig. 10. Sketch of the 3D FE hollow cylinder and the localization of sensors and incipient damage.

Table 1
Material parameters of aluminum under different conditions.

	ρ (kg/m3)	λ (GPa)	μ (GPa)	$\overline{A}$ (GPa)	$\overline{B}$ (GPa)	$\overline{C}$ (GPa)
Nonlinear Al (NAl)	2700	55.27	25.95	-351.2	-140.4	-102.8
Damaged Al (DAl)	2700	55.27	25.95	-1053.6	-421.2	-308.4

frequency. For a specific actuator-sensor path, the time T_S, corresponding to the maximum position in the resultant wavelet coefficient, is identified as the arrival time of the damage-induced nonlinear signal, as sketched in Fig. 9. Meanwhile, for the same actuator-sensor path, the propagation time of waves from the actuator (x_A, z_A), via an arbitrary inspection point (x, z) on the outer surface, to the *Sensor* (x_s, z_s) is defined as T_C:

$$T_C = \frac{\sqrt{(x_A - x)^2 + (z_A - z)^2}}{v_{surface}} + \frac{L_a}{v_{shear}} + \frac{T_{excitation}}{2} \tag{3}$$

where $v_{surface}$ and v_{shear} are the group velocity of the quasi-surface and shear waves, respectively. $T_{excitation}$ denotes the excitation signal duration. Specifically, the scattering path from the arbitrary inspection point to *Sensor* is defined as L_a. To better evaluate L_a, all positions are expressed in cylindrical coordinates. Let the arbitrary inspection point on the outer surface of the TWHC be denoted as (r_2, θ_a, z_a), and *Sensor* position as (r_1, θ_M, z_M). The total path length L_a can be determined by evaluating the corresponding integral expression.

$$L_a = \int_{r_1}^{r_2} \sqrt{1 + \left(r \cdot \frac{\theta_M - \theta_a}{r_1 - r_2}\right)^2 + \left(\frac{z_M - z_a}{r_1 - r_2}\right)^2}\, dr \tag{4}$$

where r_1 and r_2 are the inner and outer radii of the TWHC, respectively. The angles θ_a and θ_M correspond to the angular positions of the arbitrary inspection point and *Sensor*, respectively, while z_a and z_M denote their respective axial positions.

Assuming each inspection point on the outer surface of a TWHC is a possible damage location, a damage index $P_D(x,z)$ at each inspection point is defined using a symmetric exponential function, as shown in Eq. (5) [47]

$$P_D(x,z) = \sum_{i=1}^{N} e^{\left(-\frac{|T_S - T_C|}{\tau}\right)} \tag{5}$$

where τ is a decay factor which is set as 0.01 *ms* in this study. N is the total number of sensors.

3) Assigning sensor weight

In practice, when an incipient damage locates far away from a certain actuator-sensor path, the energy level of the incipient damage-induced nonlinear wave will be low and vulnerable to noise and boundary reflections. Therefore, the temporal information carried by the nonlinear signal measured by that sensor will be less reliable and less informative. In this regard, different sensors should carry different weights in the damage localization strategy according to the amplitudes of their measured nonlinear responses. Specifically, a nonlinear parameter variation (*NPV*) is defined as

$$NPV = \frac{|NP_{intact} - NP_{damage}|}{NP_{intact}} \tag{6}$$

where NP_{intact} and NP_{damage} are nonlinear parameters in the intact and damaged cases which can be defined as

$$NP = \frac{A^{NL}(2\omega)}{(A^{L}(\omega))^2} \tag{7}$$

where $A^{NL}(2\omega)$ and $A^{L}(\omega)$ are the amplitudes of the second harmonic and linear elastic wave signals, respectively, with the excitation at the fundamental frequency ω.

Furthermore, the *NPV* values of all the sensors are normalized using a *Softmax* algorithm [48], thereby quantifying the contribution of each sensor on the final damage localization results. The resultant sensor weigh (*SWi*) after the *Softmax* normalization is defined as

$$SWi = \frac{e^{NPV_i}}{\sum_{i=1}^{N} e^{NPV_i}} \tag{8}$$

This process amplifies the weight of these sensors sensitive to damage while minimizing the impact of insensitive sensors, in views of improving the damage localization accuracy.

4) Synthesizing signal features for damage localization

By synthesizing the EDZ from the *Sensor* location, $P_D(x,z)$ and *SWi* from the tests, probability of damage localization ($PDL(x,z)$) can be calculated by

$$PDL(x,z) = \sum_{i=1}^{N} P_{EDZ} \bullet P_D(x,z) \bullet SWi \tag{9}$$

It is relevant to note that the proposed method requires a baseline for the extraction of damage information. To ensure the consistency of the baselines, transducers are permanently mounted on the structures, which in the meantime can cater for the need for automatic and possibly continuous monitoring. Through the continuous comparison between the baseline response and the measurement responses, the structural health status at each measurement instant can be evaluated and therefore such method allows for the tracking of the structural health status during its operation, which is desirable in many engineering applications.

To demonstrate the superiority of the proposed localization algorithm, we define the method without SWi and EDZ as the traditional

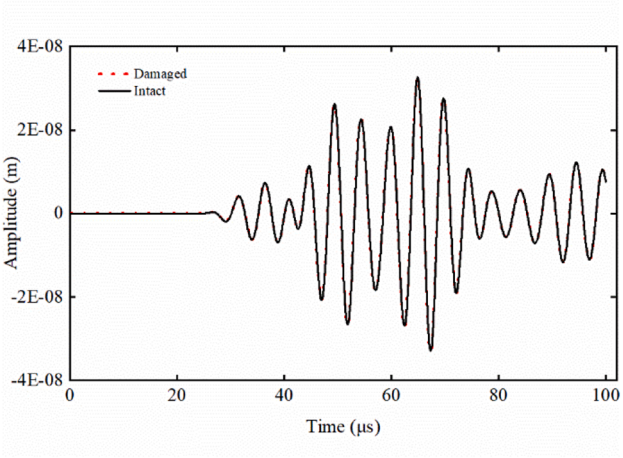

(a)

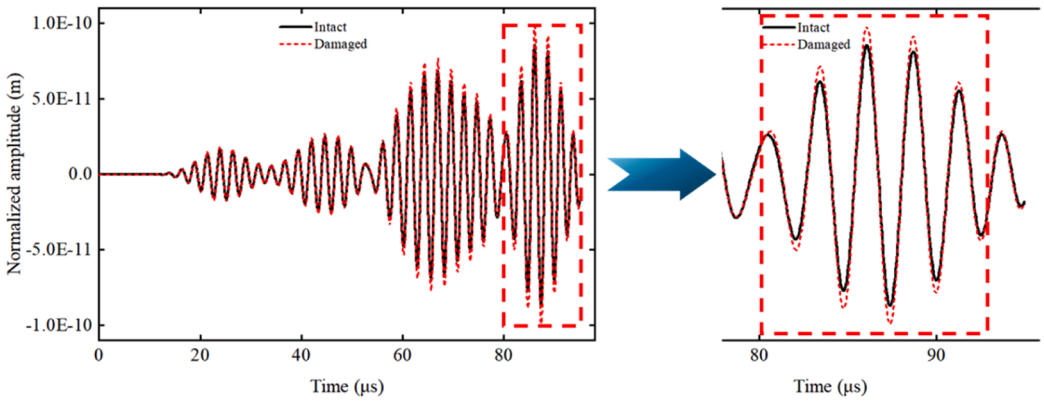

(b)

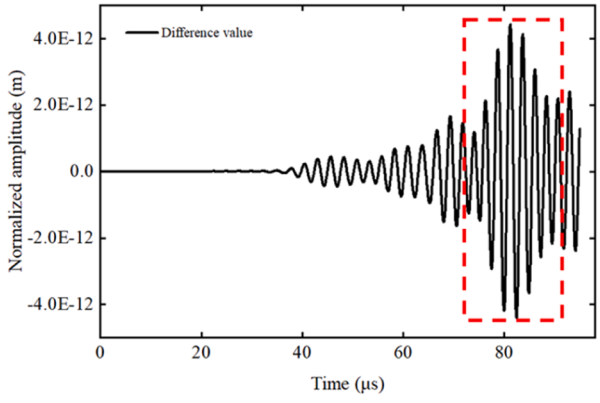

(c)

Fig. 11. FE simulated (a) linear and (b) nonlinear response signal captured at S2, (c) difference value of nonlinear response signals.

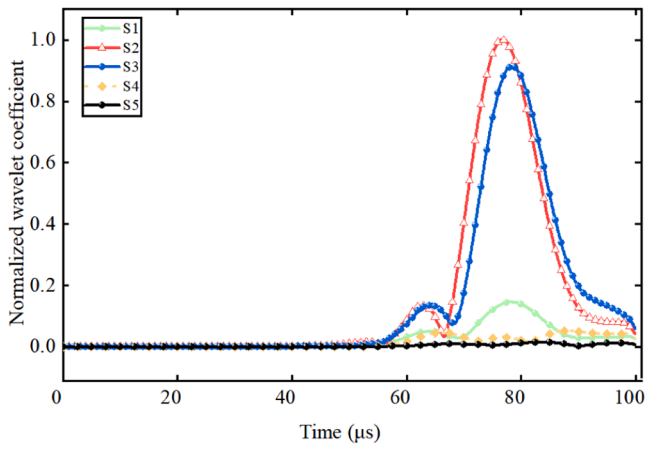

Fig. 12. FE simulated the wavelet coefficients of the incipient damage-scattered signals at sensors.

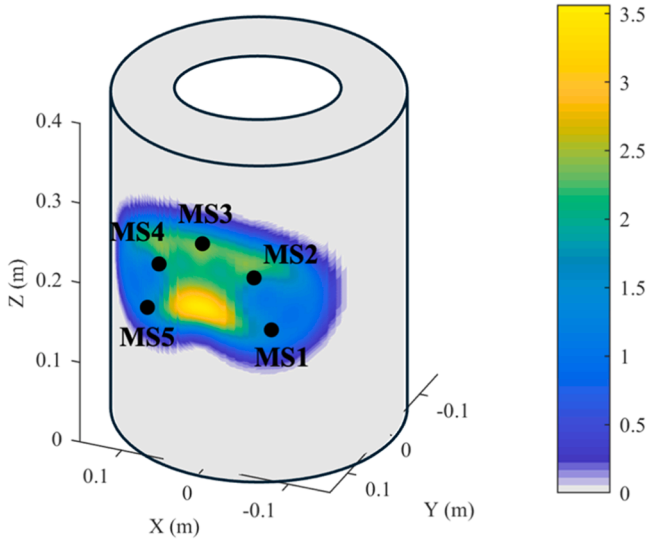

Fig. 13. Effective detection zone of the sensor network.

method ($P_D(x,z)$), which directly uses the temporal information extracted from the signal for damage localization. A comparison between the two methods is conducted in the following numerical analysis.

4. Numerical validations

Numerical simulations are carried out to validate the proposed damage localization strategy. First, an FE model is briefly described, and a signal processing method is proposed to extract damage-related signal features and temporal information. Finally, the reliability of the proposed localization algorithm is demonstrated through comparisons with the traditional method.

4.1. FE model description

A 3-D FE model is established in Abaqus/Explicit as sketched in Fig. 10. The TWHC is 400 mm long, with inner and outer radii of 100 mm and 150 mm, respectively. Both intact and damaged cases are considered. Since simulating incipient damage in numerical analysis is difficult, we mimic it through changes in material properties. The material parameters of the TWHC under different simulations scenarios are tabulated in Table 1. Nonlinear Al (NAl) stands for the intact aluminum material with weak nonlinearity through the TWHC. Damaged Al (DAl)

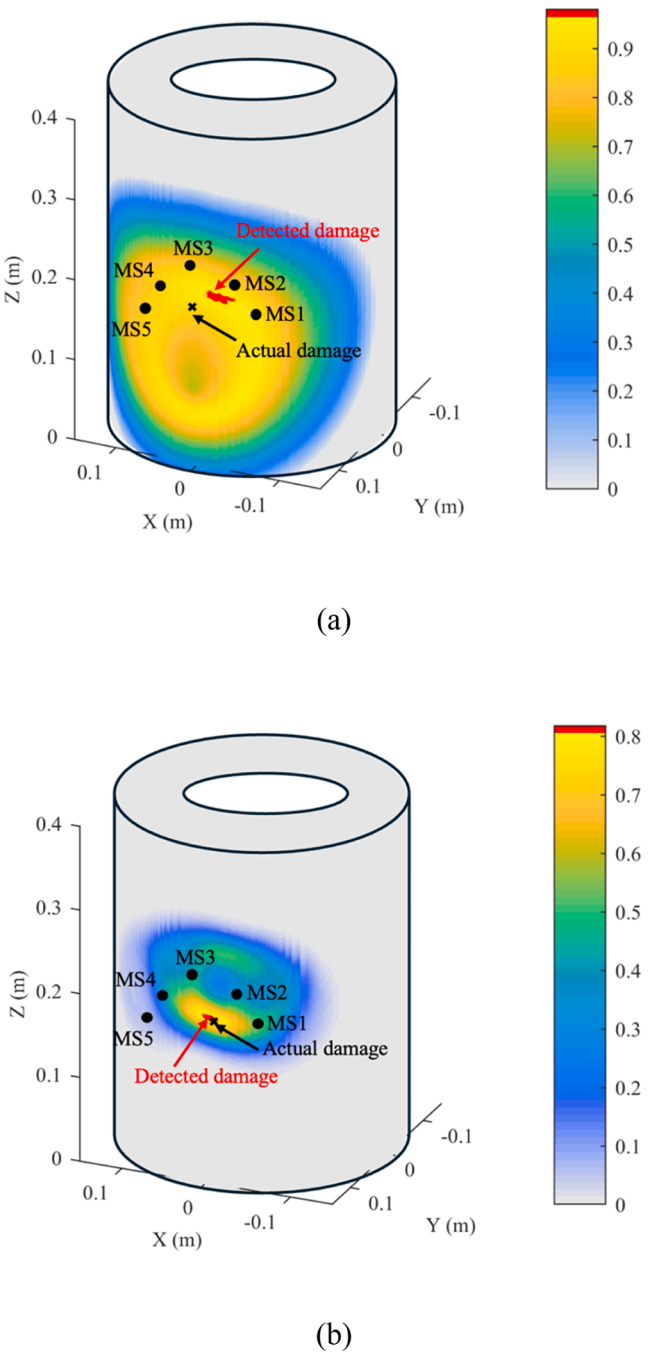

Fig. 14. Incipient damage localization results (a) without and (b) with sensor weight and EDZ.

mimics the material with incipient damage, introduced through Landau constants, which are different from NAl with the damaged area. In the former case, the TWHC is assigned with nonlinear Al (NAl) corresponding to the case of weak material nonlinearity. In the latter case, a damage zone is arbitrarily assigned over the outer surface with a size of 10 mm × 10 mm × 5 mm. The damage zone is specifically assigned with damaged Al (DAl) to mimic the material with local nonlinearity. The material nonlinearity is introduced to the model according to the Landau-Lifshitz model via the VUMAT module, as described before. It is worth noting that the Landau constants in DAl are chosen for the purpose of investigating wave propagation and do not necessarily correspond to any specific physical incipient damage [49]. In the present simulation, the DAl is assigned to the local material zone while the rest is

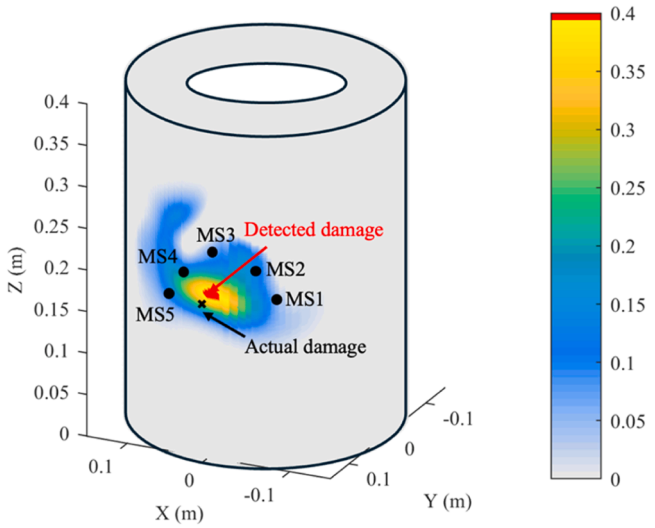

Fig. 15. Numerical validation of incipient damage localization algorithm.

assigned with NAl. The excitation is a prescribed displacement in the z direction with a 5-cycle tone burst signal at 200 kHz to mimic the action of a surface-mounted actuator. A 5-cycle tone burst excitation represents a balance between time localization and frequency resolution. It is sufficiently short to avoid excessive wave packet overlap while maintaining a narrow enough bandwidth to clearly extract second harmonic components. This excitation scheme has been widely adopted in nonlinear ultrasonic studies and was found to provide stable and repeatable nonlinear responses in both numerical simulations and experiments [50]. Similarly, the displacements in the z direction at different sensing locations are extracted as the sensor outputs. The maximum mesh size used in the FE model is 1 mm, ensuring more than 10 elements per shortest wavelength under consideration.

According to the proposed damage localization strategy, the actuator on the outer surface excites the waves, while the remaining transducers on the inner surface act as sensors. A transducer network configuration, shown in Fig. 10, is considered, which is mapped onto the outer surface of the cylinder, following the mapping scheme described before. In this process, the signal is captured with a sampling frequency of 10 MHz.

4.2. Signal processing and feature extraction

Response signals are captured before and after the introduction of the incipient damage, referred to as the intact and damaged states, respectively. Typical linear and nonlinear signals captured at sensor S2 are presented in terms of z-direction displacement in Fig. 11. It is worth noting that the linear wave responses are first examined before and after the introduction of DAl into the damage zone, indicating no noticeable changes in Fig. 11(a). This suggests that the introduced damage is indeed minor which can be considered as incipient damage. By contrast, Figs. 11(b) and 11(c) show the nonlinear responses captured at S2 with little difference. Note that a Butterworth filter is adopted with a pass-band from 350 kHz to 450 kHz to enhance the clarity of the signals. The black and red lines represent the signals in the intact and damaged status, respectively. Their difference, termed as residual nonlinear signal, is then extracted as shown in Fig. 11(c), which is induced by the incipient damage.

Complex Morlet wavelet transform is applied to extract the arrival time of the damage-induced nonlinear waves. After normalization with respect to the maximum value of S2, the magnitudes of these wavelet coefficients for sensors S1–S5 are plotted in Fig. 12. The signal amplitude captured by S2 is the largest because S2 is in closer proximity to the damage. In this figure, the time-of-flight of damage-induced nonlinear signals can be identified by the maximum normalized wavelet coefficient captured by each sensor.

4.3. Evaluation of the proposed localization method

Prior to applying the proposed damage localization strategy, it is essential to define the effective detection zone of the sensor network to ensure the accuracy and physical interpretability of subsequent localization results. As illustrated in Fig. 13, five sensors (S1–S5) are deployed on the inner surface of the TWHC structure. The color-coded region in the figure indicates the area where the sensor array exhibits sufficient sensitivity to damage, constructed through the superposition of the individual EDZs of each sensor. To ensure the reliability of the localization outcomes, all subsequent analyses are confined within this defined zone.

The proposed damage localization strategy is then applied to assess its efficacy. The location of the maximum *PDL* value is taken as the calculated damage position. Subsequently, the distance between the predicted position and the actual damage center is then calculated to quantify the localization error. To better visualize the damage localization, the localization probability imaging is mapped onto the outer surface of the TWHC.

A comparison is made between the proposed ($PDL(x,z)$) and traditional ($P_D(x,z)$) methods. Fig. 14(a) shows that the damage localization obtained using traditional method is (0.03, 0.218) m, with a 22 mm error regarding the actual damage position (0.017, 0.2) m. By comparison, the proposed method locates the damage at (0.013, 0.204) m, resulting in a 5 mm error, as shown in Fig. 14(b). Then, another case considering a different location of damage is also carried out to further

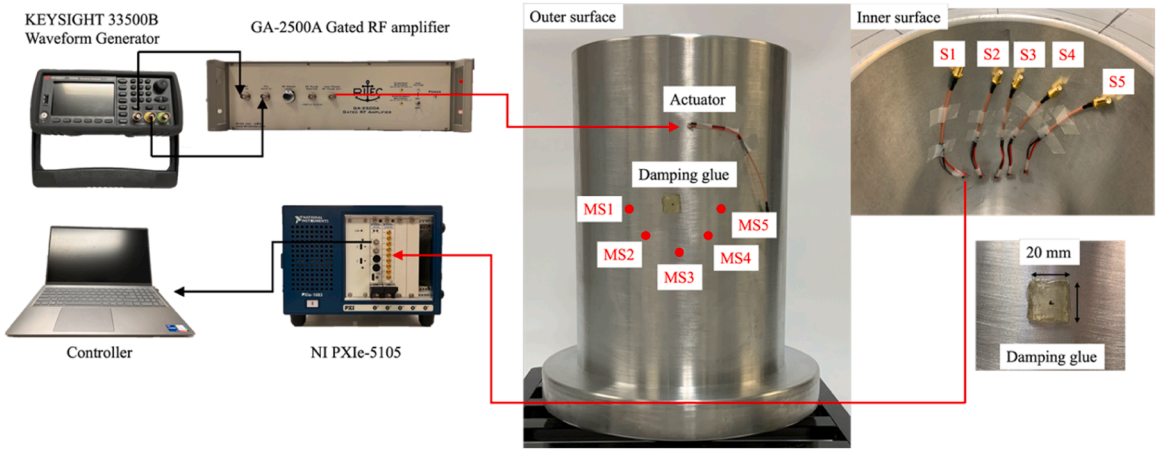

Fig. 16. Experimental setup and sensor arrangement on the outer and inner surfaces of the hollow cylinder.

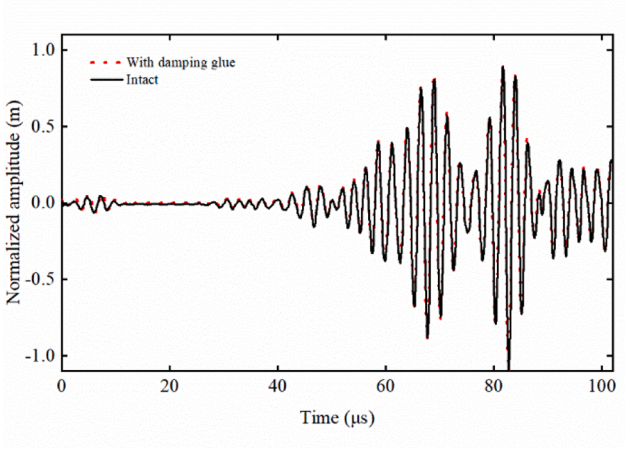

(a)

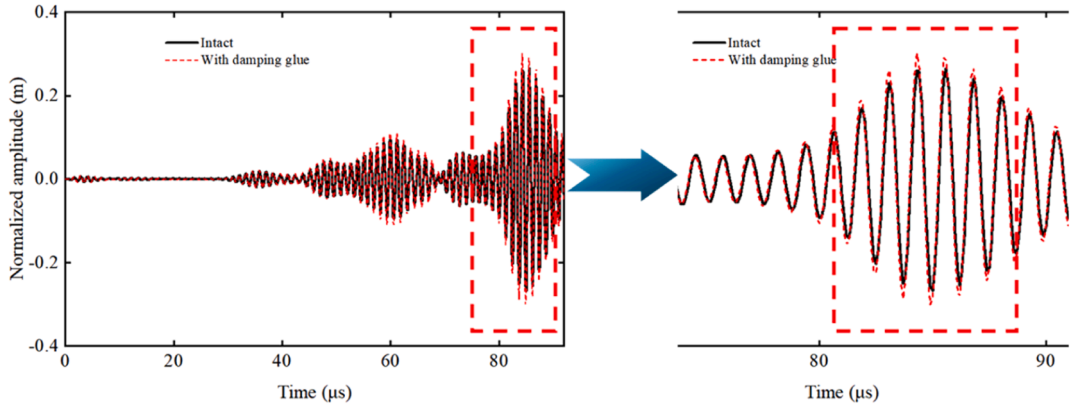

(b)

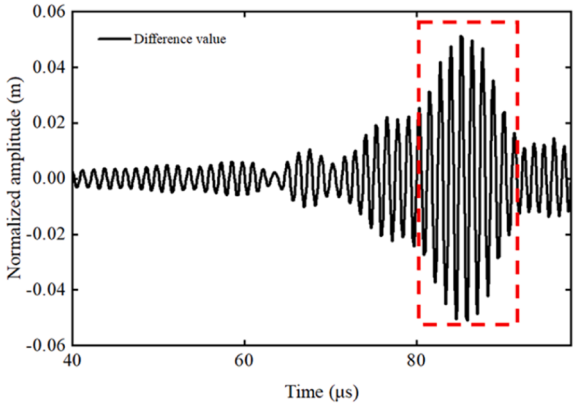

(c)

Fig. 17. (a) Experimentally measured linear response signals at S2, (b) nonlinear responses and difference signals, (c) difference value of nonlinear responses.

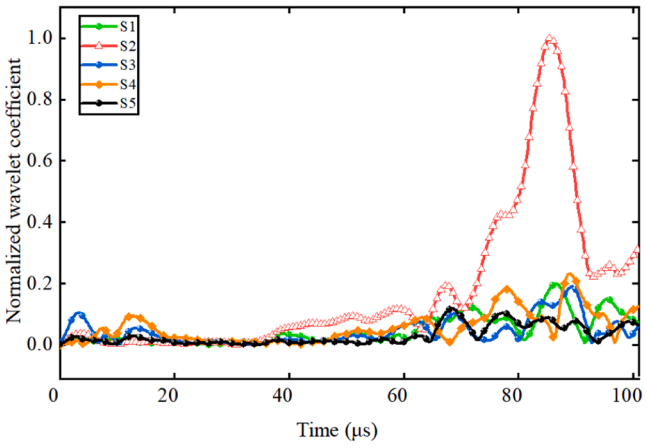

Fig. 18. Wavelet coefficients of the damage-scattered nonlinear signals at various sensors.

substantiate the above observation, resulting in a localization error of 7 mm, as shown in Fig. 15. The whole set of simulations demonstrates that the proposed strategy markedly allows for accurate damage localization.

5. Experimental validation

Experiments are finally conducted to validate the effectiveness of the proposed localization strategy. Specifically, a flexible approach for simulating incipient damage in experiments is devised, with its feasibility demonstrated.

5.1. Artificial incipient damage

In previous research, we leveraged the stamping method to create a localized plastic zone in a thick-walled beam [36]. However, generating a plastic zone through stamping on the surface of a thick-walled cylindrical structure poses considerable challenges. In traditional stamping methods, the size of the plastic deformation zone is difficult to be controlled. In addition, the plastic damage is irreversible. Once formed, the fixed location offers very limited flexibility in experiments.

To address this issue, an alternative approach is adopted here by deploying an adhesive layer on the surface of the structure to mimic a nonlinear material region. This facilitates the interrogation of damage at different locations for the purpose of validation. The adhesive layer used in the experiments is 3 M 9473 clear double-sided plastic tape, made of acrylic material. Its thickness is 0.36 mm, with an adhesion strength of 1 N/cm. The presence of the adhesive layer, through its nonlinear effects, allows the incoming quasi-surface waves to generate nonlinear components, propagating along both surface and thickness-through directions. Prior experiments were designed and conducted to verify the feasibility of the incipient damage mimicking technique, as detailed and discussed in Appendix A, in which the selection of adhesive layer thickness and a comparison of different excitation frequencies are also thoroughly discussed.

5.2. Validations of the proposed damage localization strategy

Experiments are then conducted to validate the proposed localization strategy using an aluminum hollow cylinder shown in Fig. 16 with a total length of 500 mm and inner and outer diameters of 200 mm and 300 mm, respectively. Six circular piezoelectric wafer transducers (PZTs), each with a thickness of 0.5 mm and a diameter of 6 mm, are bonded to the outer and inner surfaces of the hollow cylinder using instant glue. The measurement system operates as follows: a KEYSIGHT® 33500B waveform generator outputs an excitation signal. The

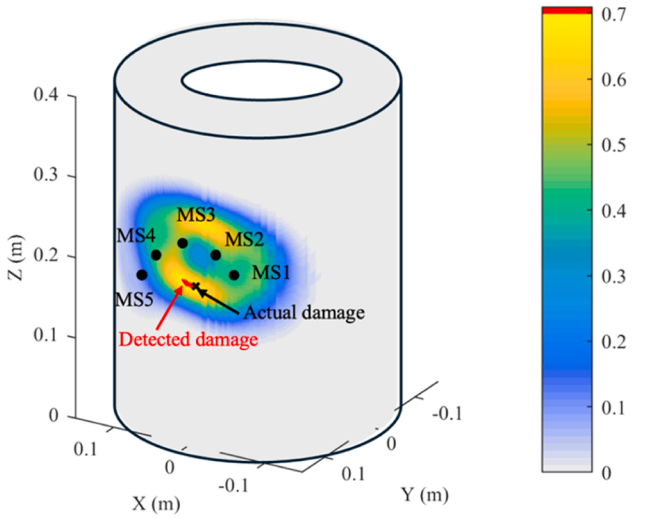

(a)

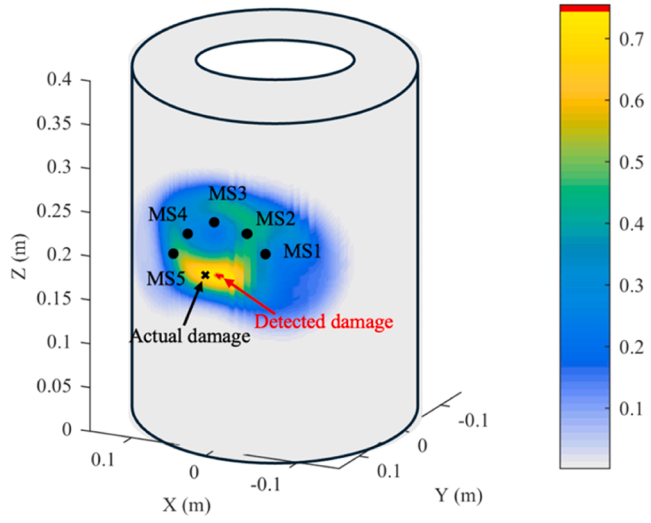

(b)

Fig. 19. Experimental damage localization results of two cases with different damage locations.

signal is then amplified by the RITEC® GA-2500A power amplifier and sent to the PZT actuator. The elastic waves are measured by the PZT sensors and recorded by the NI PXIe-5105 data acquisition module. Finally, the response signals are stored and processed by a controller.

Guided by the finite element analyses, a PZT is mounted on the outer surface of the structure as actuator, while the other five are installed on the inner surface as sensors. A 200 V, 5-cycle Hann-windowed tone burst signal, centered at 400 kHz, is utilized for excitation. The signals captured by the sensors are averaged over 100 measurements to mitigate the adverse effects of measurement noise. Additionally, a square adhesive layer, approximately 20 mm long and 0.36 mm thick, is applied to simulate an incipient damage, as depicted in Fig. 16.

In practice, due to the curvature of the cylindrical surface, the planar PZT actuator cannot achieve perfectly uniform bonding, leading to slight non-uniformity in excitation and consequently minor directional

variations in wave propagation. In principle, the direction-dependent propagation characteristics can affect the incipient damage localization results. Nevertheless, within the experimental and analytical framework adopted in this study, the influence of such spatial non-uniformity on the final results is limited. First, the analysis is performed within selected time windows to extract the target wave packets, making the approach insensitive to amplitude variations across different directions. Even when the signal energy is relatively weak in certain directions, the difference signal can still be used for damage localization as long as it can be measured. Second, multiple sensors are employed, and the information from different propagation paths is integrated during post-processing, which effectively mitigates the influence of directional variability associated with individual paths.

Similar to the finite element simulations, linear responses are examined before and after the application of the adhesive layer. A pair of typical signals are presented in Fig. 17(a). It confirms the insensitivity of the measured linear responses to the application of the adhesive layer. Extracting the second harmonic responses at sensor S2 and comparing the results in the intact and damaged states, one notices clear wave packets associated with the damage-scattered signals at 81 μs in Fig. 17 (b). By subtracting the intact signal from the damaged one, the damage-induced nonlinear signal is shown in Fig. 17(c). Complex Morlet wavelet transform was applied to extract the arrival time of the damage-induced signals. After normalization with respect to the maximum value of S2, the magnitudes of the normalized wavelet coefficients of the residual signals for sensors S1–S5 are plotted in Fig. 18. In the present study, the damage-induced nonlinear longitudinal waves that can potentially interfere with the measured signals. This effect is controlled through the time-window selection within the proposed localization framework. Specifically, the signal is first filtered using the EDZ, based on which a time window associated with the target nonlinear shear bulk waves is determined. This window is defined to capture the arrival of the dominant damage-induced nonlinear shear components, thereby minimizing the inclusion of subsequently generated longitudinal waves.

The proposed damage algorithm is then applied, resulting in the localization result shown in Fig. 19(a). The actual damage location is also marked in the side expansion map of the cylinder. The localized position is (0.012, 0.206) m, 5 mm away from the actual location (0.01, 0.202) m. Then, another case was tested with the adhesive layer glued in a different position. The resultant localization error is 8 mm, as shown in Fig. 19(b). These experimental results further confirm the efficacy of the damage localization strategy.

6. Conclusions

The present study investigates the scattering features of nonlinear bulk waves arising from the interaction between quasi-surface waves and an incipient damage on the curved surface of a TWHC. Based on the generation and propagation characteristics of nonlinear waves, an incipient damage localization strategy is proposed, with its efficacy demonstrated by both FE simulations and experiments.

Results reveal that when quasi-surface waves encounter a localized nonlinear zone on the structural surface, nonlinear shear bulk waves generate and propagate toward thickness-through direction of the TWHC till its opposite side at a predominant angle, irrespective of the curvature of the structure surface. The scattering pattern with respect to the arc roughly follows a Gaussian function. Taking this feature into account, an effective detection zone for each sensor can be established, which allows for effective assignment of the sensor weights in the proposed localization algorithm. Incorporating the effective detection zone for each sensor into the localization algorithm enable enhanced localization capability and accuracy.

The presented method offers a new avenue for incipient damage localization in a TWHC through the exploration of the nonlinear bulk wave scattering. The proposed incipient damage localization method may also offer useful guidance for engineering applications such as the early detection and localization of damage in train axles as a typical example of the TWHCs. In a broader sense, SHM of other complex thick-walled structures can also be envisaged for the safety management and maintenance of a large class of critical engineering equipment.

CRediT authorship contribution statement

Yuanman Zhang: Writing – original draft. **Shengbo Shan:** Writing – review & editing. **Li Cheng:** Writing – review & editing, Conceptualization.

Declaration of Competing Interest

The authors declare that they have no known competing financial interests or personal relationships that could have appeared to influence the work reported in this paper.

Acknowledgements

The research was funded by grants from the Research Grants Council of Hong Kong Special Administrative Region (PolyU 152013/21E), the National Natural Science Foundation of China (12302114), and the Innovation and Technology Commission of the HKSAR Government to the Hong Kong Branch of National Rail Transit Electrification and Automation Engineering Technology Research Center (K-BBY1).

Appendix A. Verifications of incipient damage generation

A series of experiments were designed and conducted to verify the reliability of the artificial incipient damage. Specifically, ultrasonic measurements were conducted on the thick-walled beam with dimension of 550 mm $\times$ 35 mm $\times$ 70 mm as illustrated in Fig. A1. A 30 mm$\times$ 16 mm$\times$ 0.5 mm piezoelectric transducer (PZT) wafer was bonded to the upper surface of each beam, 100 mm away from the beam end, for wave generation, as shown in Fig. A1. Furthermore, four square sensors (5 $\times$ 5 $\times$ 0.5 mm) were installed on the bottom surface, with Sensor S1 aligned with the location of the adhesive layer, while the remaining three sensors are spaced 40 mm apart. The dimension of the adhesive layer is 20 $\times$ 20 $\times$ 0.36 mm. The measurement system employed is same as that used in previous experiments.

First, the linear wave responses are examined before and after installing the adhesive layer. Fig. A2 shows the responses of S2, as a representative of typical signals received by the sensors. It can be observed that the linear responses hardly change after the interaction with the adhesive layer. The same observation applies to all other sensors. This proves that linear elastic waves are not sensitive to the changes brought about by the added adhesive layer, due to its incipient nature.

The second harmonic responses were then extracted using the phase-inverse method. In addition, a Butterworth filter was adopted with a passband from 750 kHz to 850 kHz to further enhance the clarity of the signals. A pair of typical responses from S2 are presented in Fig. A2. A significant increase in the nonlinear response signals occurs in S2 at 80 μs. In comparison to the intact signal, the signals triggered by the adhesive layer give rise to considerable nonlinear shear bulk waves. This further confirms that quasi-surface waves generate nonlinear shear bulk waves that propagate inward into the structure when passing through the adhesive layer, as a further evidence that the adhesive layer can indeed be employed to mimic the

incipient damage on the surface of thick-walled structures, analogous to the plastic zone generated by stamping.

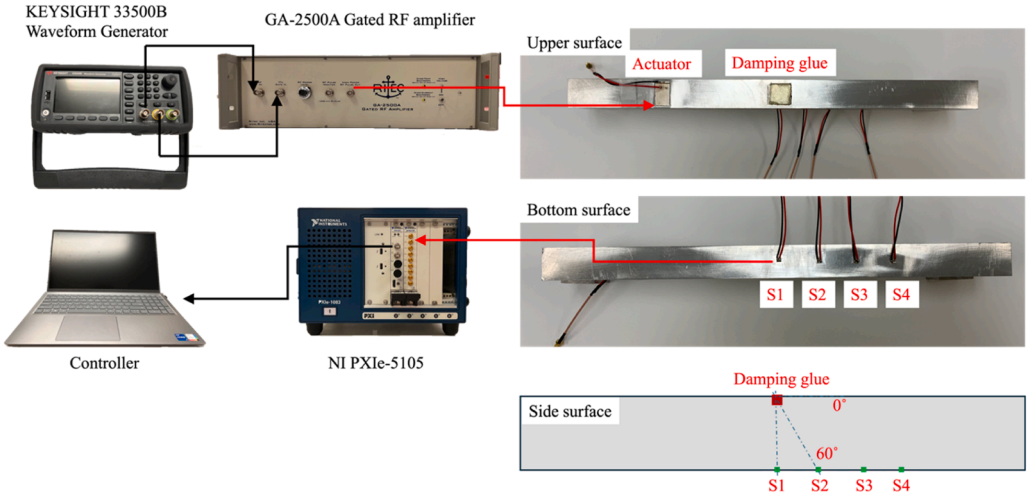

Fig. A1. Sketch of experimental set-up with damping adhesive layer.

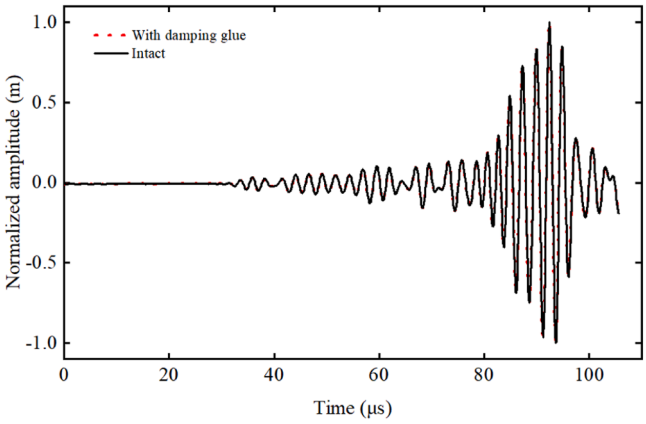

(a)

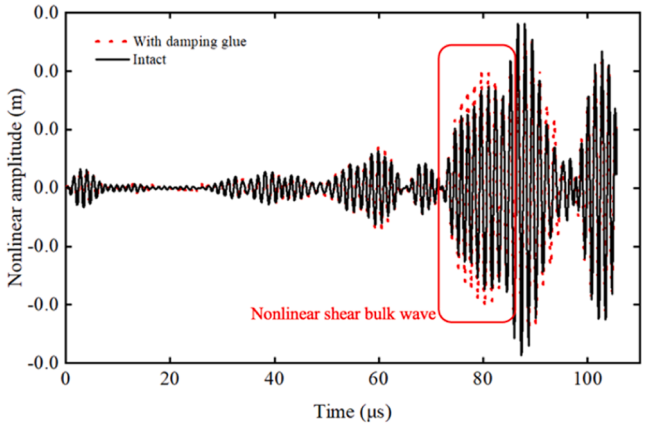

(b)

Fig. A2. Typical (a) linear and (b) nonlinear responses at sensor S2 with and without the adhesive layer.

To quantify the effect of the adhesive layer thickness on the nonlinear bulk wave signals and determine the proper experimental configuration,

multiple experiments were conducted. Firstly, the adhesive layer thickness was increasing from one layer to 3, 5, 7 and 9, while the excitation frequency was fixed at 400 kHz. The values of Nonlinear parameter variation (NPV) defined in Eq. (6) were used to quantify the changes in nonlinear responses.

The variation trends of the NPV captured by the four sensors at the bottom surface of the test beams with different adhesive layer thicknesses are shown in Fig. A3(a). It is noteworthy that, despite the differences in the layer thickness, the relative energy levels of the four sensor signals remain consistent, initially increasing and then decreasing, with S2 sensor (positioned at 60° relative to the adhesive layer) being the largest. Moreover, it is observed that with one layer, the nonlinear shear wave energy received by S2 is the most significant, indicating the optimal scattering effect.

Coming back to the one-layer configuration, the central excitation frequency of the 5-cycle tone burst was varied as 400, 600, and 800 kHz to verify the scattering properties due the adhesive layer. Following the same signal processing procedure, the NPV captured by the four sensors at different frequencies are plotted in Fig. A3(b). It follows that the variation trends of the sensors remained consistent with previous observations, with S2 still receiving the strongest nonlinear shear bulk waves. It can be concluded that, irrespective of the excitation frequency, the interaction between the quasi-surface waves and the adhesive layer generates nonlinear shear waves, scattering primarily toward 60° direction, as predicted numerically before. Additionally, the scattering directivity is more pronounced for 400 kHz excitation. Therefore, the experiments in the main context adopt the configuration of 400 kHz excitation frequency with one adhesive layer to mimic incipient damage.

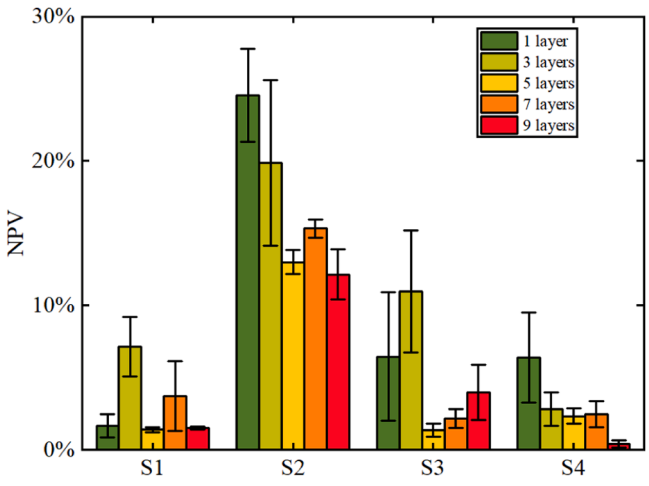

(a)

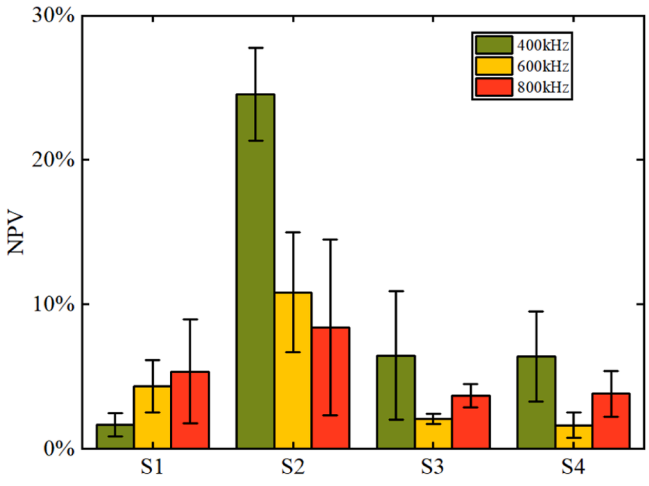

(b)

Fig. A3. Nonlinear parameter variations for (a) different layers and (b) different excitation frequency.

Data availability

Data will be made available on request.

References

[1] Makino K, Biwa S. Influence of axle–wheel interface on ultrasonic testing of fatigue cracks in wheelset. Ultrasonics 2013;53(1):239–48.
[2] Jhang K-Y. Nonlinear ultrasonic techniques for nondestructive assessment of micro damage in material: a review. Int J Precis Eng Manuf 2009;10:123–35.
[3] Chillara VK, Lissenden CJ. Review of nonlinear ultrasonic guided wave nondestructive evaluation: theory, numerics, and experiments. Opt Eng 2016;55 (1):011002 [-011002].
[4] Matlack KH, Kim J-Y, Jacobs LJ, Qu J. Review of second harmonic generation measurement techniques for material state determination in metals. J Nondestruct Eval 2015;34(1):273.
[5] Lissenden CJ, Liu Y, Rose JL. Use of non-linear ultrasonic guided waves for early damage detection. Insight-Non-Destr Test Cond Monit 2015;57(4):206–11.
[6] Mitra M, Gopalakrishnan S. Guided wave based structural health monitoring: a review. Smart Mater Struct 2016;25(5):053001.
[7] Raghavan A, Cesnik CE. In: Inman DJ, Farrar CR, Lopes Jr. V, Steffen Jr. V, editors. Lamb wave-based structural health monitoring. New York: Wiley; 2005 [2005].
[8] Willberg C, Duczek S, Vivar-Perez JM, Ahmad ZA. Simulation methods for guided wave-based structural health monitoring: a review,". Appl Mech Rev 2015;67(1): 010803.
[9] Baba S, Kondoh J. Damage evaluation of fixed beams at both ends for bridge health monitoring using a combination of a vibration sensor and a surface acoustic wave device. Eng Struct 2022;262:114323.
[10] Shi L, Cheng B, Xiang S. A fatigue crack prediction method based on inductive semi-supervised learning and Lamb-wave monitoring for orthotropic steel bridge deck. Eng Struct 2025;322:119070.
[11] Wang D, Ye L, Lu Y, Li F. A damage diagnostic imaging algorithm based on the quantitative comparison of Lambwave signals. Smart Mater Struct 2010;19(6): 065008.
[12] Liu K, et al. A novel probability-based diagnostic imaging with weight compensation for damage localization using guided waves. Struct Health Monit 2016;15(2):162–73.
[13] Xu C, Peng L, Deng M. Phased array imaging for damage localization using multi-narrowband Lamb waves. Mech Syst Signal Process 2023;190:110134.
[14] Malinowski P, Wandowski T, Trendafilova I, Ostachowicz W. A phased array-based method for damage detection and localization in thin plates. Struct Health Monit 2009;8(1):5–15.
[15] Su C, et al. Damage localization of composites based on difference signal and lamb wave tomography. Materials 2020;13(1):218.
[16] Wang W, Li H, Wang C, Zhou W, Bao Y. An improved ultrasonic computerized tomography (UCT) technique for damage localization based on compressive sampling (CS) theory. Struct Control Health Monit 2022;29(6):e2938.
[17] Polimeno MR, Roselli I, Luprano VA, Mongelli M, Tati A, De Canio G. A non-destructive testing methodology for damage assessment of reinforced concrete buildings after seismic events. Eng Struct 2018;163:122–36.
[18] Gao D, Wu Z, Yang L, Zheng Y. Guide waves-based multi-damage identification using a local probability-based diagnostic imaging method. Smart Mater Struct 2016;25(4):045009.
[19] Gao W, Zhang M, Zhang C. Load-induced crack characterization in concrete beam based on novel bidirectional sensing fused probability imaging algorithm. Eng Struct 2025;342:120909.
[20] Nzouatchoua CB, et al. Damage localization on composite structures based on the delay-and-sum algorithm using simulation and experimental methods. Sensors 2023;23(9):4368.
[21] Zhang M, Zhou D, Sun X, Yang Z, Kong Q. Enhanced damage localization in plate-like concrete structures leveraging modified delay-and-sum method. Struct Health Monit 2024 [14759217241267771].
[22] Zhu J, Li W, Mu K, Zhang X, Zhao X. An automatic arrival time picking algorithm of ultrasonic waves for concrete crack depth detection. Eng Struct 2025;328:119729.
[23] Leonard KR, Hinders MK. Lamb wave tomography of pipe-like structures. Ultrasonics 2005;43(7):574–83.
[24] Tyutekin V. Helical waves of an elastic cylindrical shell. Acoust Phys 2004;50(3): 273–7.
[25] Tyutekin V, Boiko A. Helical normal waves near a cylindrical cavity in an elastic medium. Acoust Phys 2010;56(2):141–4.
[26] Zhu Y, Hu Y, Li F, Abbas S, Bao W, Su W. Internal damage localization for large-scale hollow cylinders based on helical sensor network. Struct Health Monit 2023; 22(4):2469–80.
[27] Hu Y, et al. Bayesian hierarchical hyper-Laplacian priors for high-resolution defect imaging in pipe structures. Mech Syst Signal Process 2024;214:111351.
[28] Andreades C, Fierro GPM, Meo M. A nonlinear ultrasonic modulation approach for the detection and localisation of contact defects. Mech Syst Signal Process 2022; 162:108088.
[29] Andreades C, Fierro GPM, Meo M. A nonlinear ultrasonic SHM method for impact damage localisation in composite panels using a sparse array of piezoelectric PZT transducers. Ultrasonics 2020;108:106181.
[30] Yan X, Wang H, Fan X. Research progress in nonlinear ultrasonic testing for early damage in metal materials. Materials 2023;16(6):2161.
[31] Yang D, Zhang B, Cai R, Hong X. Multiple domain dynamic feature adaption transfer learning method for stranded wires health monitoring under variable vibration working conditions using laser-generated ultrasonic guided wave. Eng Struct 2023;297:117013.
[32] Boccardi S, Callá DB, Ciampa F, Meo M. Nonlinear elastic multi-path reciprocal method for damage localisation in composite materials. Ultrasonics 2018;82: 239–45.
[33] Chen H, Gao G, Hu N, Deng M, Xiang Y. Modeling and simulation of frequency mixing response of two counter-propagating Lamb waves in a two-layered plate. Ultrasonics 2020;104:106109.
[34] Zhang Y, Shan S, Cheng L. Elastic wave propagation in thick-walled hollow cylinders for damage localization through inner surface sensing. Ultrasonics 2023; 133:107027.
[35] Shao S, Xia R, Li Z. Tunable piezoelectric metasurface for manipulating multi-mode guided waves in plate. Eng Struct 2022;270:114917.
[36] Zhang Y, Shan S, Cheng L. Local plasticity-induced nonlinear surface wave scattering in thick-walled structures. Ultrasonics 2024:107363.
[37] Rahman Z, Ohba H, Yoshioka T, Yamamoto T. Incipient damage detection and its propagation monitoring of rolling contact fatigue by acoustic emission. Tribol Int 2009;42(6):807–15.
[38] Shan S, Cheng L, Wen F. Design of nonlinear-Lamb-wave-based structural health monitoring systems with mitigated adhesive nonlinearity. Smart Mater Struct 2018;27(10):105006.
[39] Shan S, Cheng L. Mode-mixing-induced second harmonic A0 mode Lamb wave for local incipient damage inspection. Smart Mater Struct 2020;29(5):055020.
[40] Wen F, Shan S, Cheng L. Third harmonic shear horizontal waves for material degradation monitoring. Struct Health Monit 2021;20(2):475–83.
[41] Yuan H, Chen J, Krompholz K, Wittmann FH. Investigations of size effects in tensile tests based on a nonlocal micro-mechanical damage model. Comput Mater Sci 2003;26:230–43.
[42] Ju J, Lee X. Micromechanical damage models for brittle solids. Part I: tensile loadings. J Eng Mech 1991;117(7):1495–514.
[43] Shan S, Cheng L, Li P. Adhesive nonlinearity in Lamb-wave-based structural health monitoring systems. Smart Mater Struct 2016;26(2):025019.
[44] Ahrendt P. The multivariate gaussian probability distribution. Tech Univ Den Tech Rep 2005;203.
[45] Gong C, et al. Dual-frequency acousto-ultrasonic sensing of impact damage in composites for mitigating signal instability. Struct Health Monit 2022;21(2): 282–97.
[46] Gong C, Wu Q, Zhang H, Li P, Xiong K. Numerical simulation of Lamb wave sensing of low-velocity impact damage in composite laminate. Compos Struct 2022;279: 114844.
[47] Huo H, He J, Guan X. A Bayesian fusion method for composite damage identification using Lamb wave. Struct Health Monit 2021;20(5):2337–59.
[48] M. Wang, S. Lu, D. Zhu, J. Lin, Z. Wang. A high-speed and low-complexity architecture for softmax function in deep learning. In: Proceedings of the 2018 IEEE Asia Pacific conference on circuits and systems (APCCAS). IEEE; 2018. p. 223–6.
[49] Xiang Y, Deng M, Xuan F-Z, Liu C-J. Experimental study of thermal degradation in ferritic Cr–Ni alloy steel plates using nonlinear Lamb waves. Ndt E Int 2011;44(8): 768–74.
[50] K.M. Qatu, A. Abdelgawad, K. Yelamarthi. Structure damage localization using a reliable wave damage detection technique. In: Proceedings of the 2016 international conference on electrical, electronics, and optimization techniques (ICEEOT). IEEE; 2016. p. 1959–62.